PHYSICAL REVIEW D

PARTICLES AND FIELDS

THIRD SERIES, VOL. 8, NO. 7 1 October 1973

Compilation of Data for $\pi^{\pm}p$ Inclusive Reactions at 8 and 18.5 GeV/c. I. Single-Particle Distributions*

J. T. Powers,† N. N. Biswas, N. M. Cason, V. P. Kenney, and W. D. Shephard

Department of Physics, University of Notre Dame, Notre Dame, Indiana 46556

(Received 20 April 1973)

Production of negative pions in the single-particle inclusive reactions $\pi^- + p \to \pi^- +$ anything at 8 and 18.5 GeV/c and $\pi^+ + p \to \pi^- +$ anything at 18.5 GeV/c is analyzed in terms of different sets of kinematic variables for various reference frames. Proton fragmentation is studied in terms of (P_l, P_T^2) in the lab system. In the c.m. system, the variables (x, P_T^2) are useful for the study of incident-particle effects and the energy dependence of cross sections. The variables (y, P_T^2) allow a more detailed study of the kinematic region near $x = 0$. The variables (y_r, P_T^2) are particularly useful in that the reduced rapidity y_r has a fixed kinematic boundary independent of s and P_T^2. Topological cross sections and multiplicity moments are presented.

I. INTRODUCTION

In the study of hadron-hadron interactions, particularly at very high energies, there has been considerable interest in the description of inclusive reactions of the type $a + b \to c +$ anything, $a + b \to c_1 + c_2 +$ anything, etc. While the applicable phenomenological theory is generally asymptotic in character, and in principle, at least, useful at only the highest energies, one is interested in knowing to what extent the description of inclusive reactions changes as the center-of-mass energy is varied from "conventional" accelerator energies up to the asymptotic limit.

The conscientious experimenter is faced, at the outset, with the problem that there is as yet no clearcut choice to be made in the set of variables with which to present the data, or even in the reference frame in which the interaction is to be described. Different phenomenological models favor different choices. There is a real possibility that the experimenter may inadvertently bias his treatment of the subject by his own choice of variables.

We have already extracted a certain amount of information[1-4] from the Notre Dame $\pi^{\pm}p$ inclusive-reaction sample. In the interests of making these data available for wider use, the present paper is intended to provide an analysis of the production of negative pions in the single-particle inclusive reactions

$$\pi^- + p \to \pi^- + \text{anything} \tag{1}$$

at 8.05 and 18.5 GeV/c, and

$$\pi^+ + p \to \pi^- + \text{anything} \tag{2}$$

at 18.5 GeV/c in terms of different sets of kinematic variables. The analysis of the two-particle inclusive reactions and the correlations between the produced particles will be presented in a subsequent paper.

In Sec. II we discuss the kinematic properties of the different variables and their relationships. In Sec. III, we present the experimental procedure used to obtain our samples of data. We present cross sections and multiplicity moments in Sec. IV and compare our values with results published at other energies. This allows us to check the consistency of our data with those of previously pub-

lished experiments. In Sec. V we present distributions for single-pion production in terms of the different variables, and in Sec. VI we discuss our results.

II. KINEMATICS AND VARIABLES

We have studied the kinematic properties of reactions (1) and (2) in terms of several different variables. The basic quantity of interest which describes the single-particle inclusive reaction is the invariant differential cross section

$$f(\vec{p}, s) = E \frac{d\sigma}{d^3p},$$

where s is the square of the total c.m. energy and $(\vec{p}, E)$ is the four-momentum of the produced particle. For unpolarized beam and target, $f(\vec{p}, s)$ is a function of s and two other independent variables which may be chosen from among several sets. The sets of kinematic variables used in this paper are (P_l, P_T^2), (x, P_T^2), (y, P_T^2), and (y_r, P_T^2), where P_l is the component of momentum along the direction of the beam in the laboratory frame, x is the Feynman scaling variable, y is the rapidity, y_r is a "reduced" rapidity, and P_T^2 is the square of the transverse momentum for the produced particle.

For comparison with models of inclusive reactions, the physical quantities are examined in the reference frame for which theoretical predictions are made. Fragmentation models lead to predictions about the distribution of particles whose momenta remain finite in the rest frame of the target or projectile as $s \to \infty$. Thus, the appropriate variables for the study of target fragmentation are P_l and P_T^2. Models which make predictions about the distribution of particles whose momenta remain finite in the over-all c.m. frame as $s \to \infty$ are better studied in terms of x and P_T^2, where $x = P_l^{\text{c.m.}} / P_0^{\text{c.m.}}$ with $P_l^{\text{c.m.}}$ and $P_0^{\text{c.m.}}$ defined as the c.m. longitudinal momentum of the emitted particle and the c.m. momentum of the projectile.

The limited range of x, namely $-1 < x < 1$ independent of c.m. energy, makes this an attractive variable. As we go to higher energies, however, small but finite momenta in the c.m. system are mapped into a progressively smaller region of x near $x = 0$. Thus x is not suited for a detailed study of this region.

The rapidity variable y has the advantage [5-7] of expanding the region near $x = 0$ and thus allowing a detailed study of this central region. The rapidity variable is related to the longitudinal momentum P_l in any reference frame

$$y = \tfrac{1}{2} \ln\left(\frac{E + P_l}{E - P_l}\right)$$

$$= \ln\left(\frac{E + P_l}{\mu}\right),$$

where the longitudinal mass μ is defined as $\mu = (P_T^2 + m^2)^{1/2}$ with m being the mass of the produced particle. Then $P_l = \mu \sinh y$ and $E = \mu \cosh y$. Rapidity may be evaluated in any reference frame with the added feature that, under a longitudinal Lorentz transformation, $y \to y + \text{constant}$. Thus distributions of rapidity in all longitudinal frames are related by a simple shift in scale. In this paper we present distributions as a function of the c.m. rapidity. The allowed range of y is dependent on s and on the mass of the particle. It is also important to remember, as has been emphasized by Van Hove,[8] that y is not a pure longitudinal variable, but depends on both P_l and P_T^2. In fact, for light particles (e.g., pions) the rapidity varies quite rapidly with P_T^2 when $P_T^2 \gtrsim m^2$. The kinematically allowed region in y for the asymptotic limit ($s \gg m_a^2$ and m_b^2) has a width

$$Y = \ln(s/\mu^2).$$

Thus, the range of a y distribution varies with the type of particle observed and with s, but not with the nature of the beam or target particle.

We can define a reduced rapidity y_r in the c.m. frame, similar to that suggested by Frazer *et al.*[9] for the laboratory frame, which avoids some of the difficulties associated with the use of y. In the c.m. system, y is restricted to the range $-\frac{1}{2}Y \leq y \leq +\frac{1}{2}Y$ at asymptotic s. Thus it is convenient to define y_r to be

$$y_r = 2y/Y,$$

so that the range of y_r is $-1 \leq y_r \leq 1$ for any allowed value of transverse momentum and is independent of the mass of the particle. This reduced rapidity retains the convenient properties of y without the strong dependence on P_T, but has a property similar to x in that momenta which are finite in the rest frame of the target (projectile) are mapped into a single point at $y_r \approx -1(+1)$ for very large s.

In Fig. 1 we show the allowed kinematic regions for the production of a single pion in reactions (1) and (2) at 18.5 GeV/c, in terms of (y_r, P_T^2), (y, P_T^2), (x, P_T^2), and (P_l, P_T^2). We note that the kinematically allowed region in the (y, P_T^2) plot shown by the solid lines in Fig. 1(b) narrows very rapidly as P_T^2 increases, while the allowed widths in terms of x, P_l, and y_r change only gradually with P_T^2. The figure shows how lines of constant y_r map into y, x, and P_l. Here y_r, y, and x are

c.m. variables, while P_l refers to the laboratory reference frame. Figure 1(a) shows lines of constant y_r as a function of P_T^2 separated by an interval of $\Delta y_r = 0.2$. Figures 1(b), 1(c), and 1(d) show the corresponding contours in terms of y, x, and P_l. As shown in Fig. 1(b), for small c.m. longitudinal momenta (approximately between lines D and F), y is approximately independent of P_T^2. For larger values of $|y|$ there is a much stronger dependence of P_T^2. In Fig. 1(c) we see that the same region of y_r is concentrated into a smaller range of x around $x = 0$, especially for small P_T^2. The disadvantage of using the variable x in a study of this central region is thus illustrated. Figure 1(d) shows that the region $y_r < 0$ maps into a very small range of P_l near the minimum value. In this region lines of constant y_r also correspond to fairly constant values of P_l. Thus one can study the target fragmentation region using either the P_l or y_r variables. Figure 1 is useful in visualizing the relationship of a phase-space element in one set of variables to the corresponding element in another set.

III. EXPERIMENTAL PROCEDURE

The data for this experiment were obtained at Brookhaven National Laboratory in several runs of the 80-in. hydrogen bubble chamber exposed to beams of pions from the Alternating Gradient Synchrotron (AGS). A total of 152 000 pictures of π^+p interactions was obtained using the rf-separated π^+ beam with a nominal momentum of 18.5 GeV/c (measured to be 18.465 ± 0.092 GeV/c). An unseparated π^- beam of nominal momentum 18.5 GeV/c (measured to be 18.480 ± 0.092 GeV/c) was used to obtain 170 000 photographs. An earlier exposure of 50 000 pictures taken with a π^- beam of nominal momentum 8.05 GeV/c (measured to be 8.050 ± 0.040 GeV/c) was also used in the present analysis. The total 8.05-GeV/c exposure was included in our study, while only 44% of the π^+p pictures and 30% of the π^-p pictures at 18.5 GeV/c were used.

The 18.5-GeV/c π^+p and π^-p pictures were scanned for all events which produced at least one negative secondary. Thus π^-p events were recorded if they had two or more prongs while four or more prongs were required in π^+p interactions. Since measurements of 2-prong, 4-prong, and 8-prong events at 8.05 GeV/c already existed an additional scan was made for events with 6 prongs and ≥ 10 prongs in the whole sample. A sample of 10% of the 8.05-GeV/c film was scanned separately for all events to determine relative numbers of events of different multiplicities in a consistent fashion.

Throughout our analysis we assume that all of the observed negative particles are pions except those which are obviously strange particles from their decay. The ratio of $\pi^+\pi^- : K^+K^- : p\bar{p}$ production in the four-body final state for π^+p and π^-p interactions at 18.5 GeV/c has been independently determined[10] to be 100 : 3 : 1. We estimate the non-

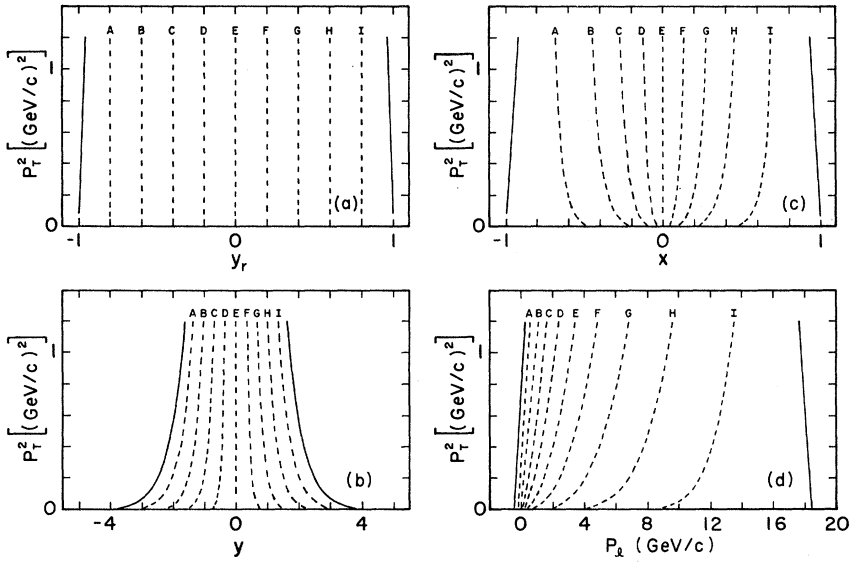

FIG. 1. Allowed kinematic regions for a single pion produced in the reaction $\pi + p \rightarrow \pi +$ anything at 18.5 GeV/c. Solid lines represent the kinematic boundaries of phase space. Dashed lines of constant y_r, denoted A, B, ... I, are mapped into those with the same labels upon transformation from y_r to y, y_r to x, and y_r to P_l, as discussed in the text.

pion contamination in our samples to be at most a few percent.

For each event in this experiment, measurements were made of the beam track and of all negative tracks which were not obvious strange particles. All events were measured including those with obviously associated neutral strange particles. The events were measured on three film-plane and two image-plane machines and were reconstructed using the geometry program HAG (the Notre Dame version of HGEOM[11]).

The final result of the reconstruction process was a "four vector" tape containing the vector momenta of all negative tracks in each event for which all tracks were successfully reconstructed. The momentum of the beam track was assumed to be the nominal beam momentum corrected for energy loss in the chamber. Since the relevant variables for inclusive reactions such as P_T^2 often are quite sensitive to the direction of the incident track at the vertex, the beam angles were determined from a weighted average of the measured values in an event together with average values determined for long well-measured beam tracks. Vector momenta for secondary tracks were obtained from the geometry program without further kinematic constraints.

The relative numbers of events of different multiplicity in our final sample can differ from relative numbers of events observed in scanning due to measuring difficulties and failures in reconstruction. To correct for this in determining final distributions we have weighted each event so that the number of events for each charge multiplicity is equal to the number found in the inclusive scan after correction for scanning efficiencies etc. A study of remeasured events at 18.5 GeV/c showed that, as might be expected, tracks of high momentum (nearly straight tracks) were more likely to fail in reconstruction. To correct for this bias, events with tracks which failed in reconstruction on first measurement but which were successfully reconstructed after careful remeasurement were assigned different weights than events of the same topology which were successfully reconstructed from initial measurements. Further details of the procedure used in obtaining final distributions are presented elsewhere.[12]

In order to obtain distributions which are normalized to absolute cross sections, we have calculated the values of the cross section per event in the inclusive scans by normalizing to independent determinations of the 4-prong cross sections. The values are: $(2.585 \pm 0.065) \times 10^{-3}$ mb/event for 8.05 GeV/c $\pi^- p$, $(0.4472 \pm 0.0126) \times 10^{-3}$ mb/event for 18.5 GeV/c $\pi^- p$, and $(0.2474 \pm 0.0088 \times 10^{-3}$ mb/event for 18.5 GeV/c $\pi^+ p$.

Our final samples of negative secondary tracks with measured momenta include 62 224 tracks for 8.05 GeV/c $\pi^- p$ interactions, and 100 911 and 101 917 tracks for 18.5 GeV/c $\pi^- p$ and $\pi^+ p$ interactions, respectively.

IV. GENERAL PROPERTIES OF πp INTERACTIONS

A. Topological Cross Sections and Multiplicity Distributions

We have obtained topological cross sections in a consistent manner for 8.05 and 18.5 GeV/c $\pi^- p$ and 18.5 GeV/c $\pi^+ p$ interactions, by normalizing to independent determinations of the 4-prong topological cross sections. (Special care was taken to insure that scanning biases were minimized and good statistical accuracy was obtained for these determinations.) Corrections have been made for scanning and measuring efficiencies for different topologies.

Topological cross sections for the different charged multiplicities are shown in Table I. We note that the 18.5-GeV/c $\pi^+ p$ and $\pi^- p$ cross sections at a given multiplicity n are equal within errors for $n \geq 4$. Also, although the total inelastic cross sections at 18.5 GeV/c are nearly equal, the cross sections for producing a negative pion inelastically differ by about 4 mb between $\pi^- p$ and $\pi^+ p$ interactions.

The variation of the partial cross sections with total c.m. energy, $s^{1/2}$, is shown in Fig. 2. Here we have plotted the fraction of the total inelastic cross section for each charge multiplicity so that one may see how the mixture of multiplicities changes with energy. We note that our cross sections at 8.05 GeV/c ($s^{1/2} = 4.00$ GeV) and 18.5 GeV/c

TABLE I. Cross sections.

Number of charged secondaries	8.05-GeV/c $\pi^- p$ σ (mb)	18.5-GeV/c $\pi^- p$ σ (mb)	18.5-GeV/c $\pi^+ p$ σ (mb)
0	0.80 ± 0.30 [a]	0.35 ± 0.08	...
2	13.80 ± 0.51	8.72 ± 0.34	7.20 ± 0.60 [a]
4	10.28 ± 0.20	9.17 ± 0.25	9.04 ± 0.32
6	2.70 ± 0.11	5.26 ± 0.16	5.55 ± 0.20
8	0.227 ± 0.025	1.58 ± 0.05	1.64 ± 0.06
10	0.005 ± 0.003	0.266 ± 0.013	0.285 ± 0.013
12	...	0.029 ± 0.004	0.031 ± 0.003
14	...	0.0031 ± 0.0012	0.0030 ± 0.0008
16	...	0.0004 ± 0.0004	...
Total	27.81 ± 0.63	25.38 ± 0.46	23.75 ± 0.71
Elastic	5.05 ± 0.30 [a]	4.21 ± 0.17 [a]	4.07 ± 0.30 [a]
Inelastic	22.76 ± 0.70	21.17 ± 0.49	19.68 ± 0.77
Inelastic π^-	21.96 ± 0.63	20.82 ± 0.49	16.55 ± 0.38

[a] The cross section for this channel is estimated from the literature.

($s^{1/2}$ = 5.96 GeV) are in good agreement with the data at other energies, taken from the literature. Over the presently available energy range the inelastic 2-prong cross section is falling rapidly while higher-prong (6-prong and higher) cross sections are rising, resulting in the observed slow variation in total cross section. In π^-p interactions, the total cross section for inelastic π^- production is also slowly varying. This is not the case, however, in π^+p interactions. Since the 2-prong cross section does not contribute, the total cross section for producing negative pions is rapidly rising. The charged multiplicity distributions for different values of incident beam momentum are shown in Fig. 3. The distributions become broader as the incident momentum increases.

B. Multiplicity Moments

An important quantity in multiparticle reactions, which is related to the above multiplicity distributions, is the average number of particles produced as a function of the total c.m. energy. The behavior of the mean multiplicity as a function of s is an important prediction of various models. In addition, the rate at which other moments increase with s may provide even more crucial tests, as has been pointed out by numerous authors.[13]

We have calculated the multiplicity moments, using inelastic cross sections only, for π^-p interactions at 8.05 and 18.5 GeV/c and π^+p interactions at 18.5 GeV/c. In Table II we present multiplicity moments for n_{ch}, the total number of charged secondaries, and for n_- (n_+), the number of negative (positive) secondaries. In order to study the s dependence of these moments, we have calculated values at other energies using the topological cross sections shown in Fig. 2. In Fig. 4, we have plotted $\langle n_{ch} \rangle$ as a function of $\ln E^{c.m.}$, where $E^{c.m.} = s^{1/2}$. The straight lines represent the best fit to the expression

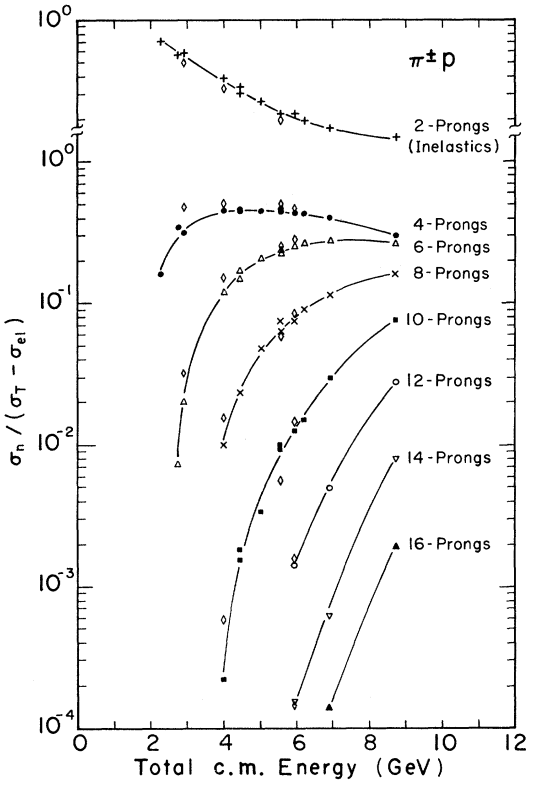

FIG. 2. Fraction of the total inelastic cross section contributed by the various charge multiplicities as a function of the total c.m. energy. Data are shown for π^-p 2-prong inelastic (+), 4-prong (●), 6-prong (△), 8-prong (X), 10-prong (■), 12-prong(○), 14-prong (▽), and 16-prong (▲) interactions. Also shown are the corresponding data for π^+p interactions (◇). The curves through the π^-p data are shown to guide the eye.

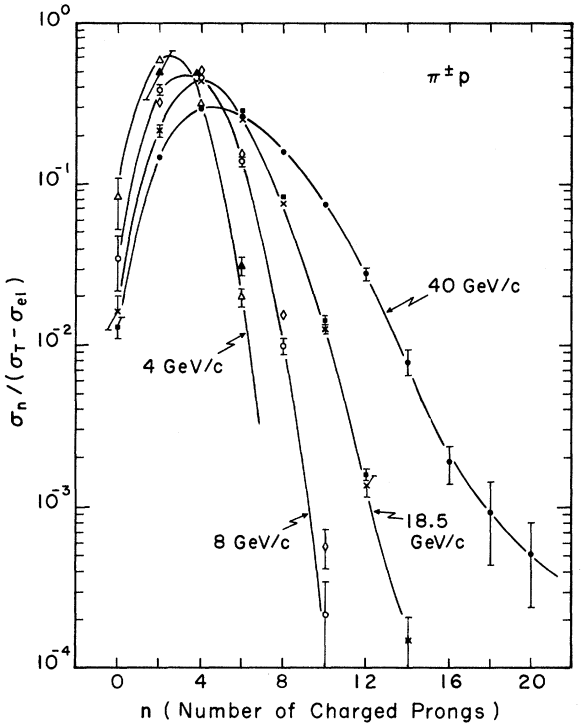

FIG. 3. Fraction of the total inelastic cross section contributed by the various charge multiplicities as a function of the number of charged prongs in the final state. Data are shown for π^-p interactions at 4 GeV/c (△), 8.05 GeV/c (○), 18.5 GeV/c (X), 40.0 GeV/c (●), and for π^+p interactions at 4 GeV/c (▲), 8 GeV/c (◇), and 18.5 GeV/c (■). The curves through the π^-p data are shown to guide the eye. [The 40-GeV/c data are from A. Abdurakhimov *et al.*, JINR Dubna Report No. P1-6277, 1972 (unpublished).]

$$\langle n_{\rm ch}\rangle = A + B \ln E^{\rm c.m.}$$

for values of $E^{\rm c.m.} \geq 4$ GeV. The dashed curves represent best fits to the power-law expression

$$\langle n_{\rm ch}\rangle = A (E^{\rm c.m.})^B$$

over the same energy range. The parameters for these fits are given in Table III. Although the data slightly favor the power-law fit, the $\ln E^{\rm c.m.}$ behavior also fits the data well.

Diffraction-dissociation and multiperipheral models both predict that $\langle n_{\rm ch}\rangle$ should increase as $\ln s$. In fact, any theory which predicts a central plateau in rapidity which scales at asymptotic s will lead to a $\ln s$ dependence.[14] Berger and Krzywicki[15] have suggested that the $\ln s$ behavior may not become evident until much higher energies and that, at low energies, a power-law form of $s^{1/3}$ or $s^{1/4}$, might be expected on the basis of kinematics. Our fits are consistent with either of these power-law forms. We note that the energy dependence of $\langle n_{\rm ch}\rangle$ is very similar for inelastic πp and pp interactions.

We next consider multiplicity moments for $x>0$ and $x<0$ in the c.m. system. Quigg, Wang, and Yang[16] emphasize the importance of these moments. They suggest that the left-hand ($x<0$) and right-hand ($x>0$) hemispheres in the center of mass are independent, the left (L) hemisphere containing fragments of the left-hand incident particle and the right (R) hemisphere containing the fragments of the right-hand incident particle. The multiplicity in each hemisphere is assumed to be independent of the multiplicity in the other, and large fluctuations in the moments for either hemisphere may be large as s is varied. We calculate values of the right and left multiplicity moments[17] for the inelastic production of negative pions. Table IV shows values of these moments for our data at 8.05 and 18.5 GeV/c.

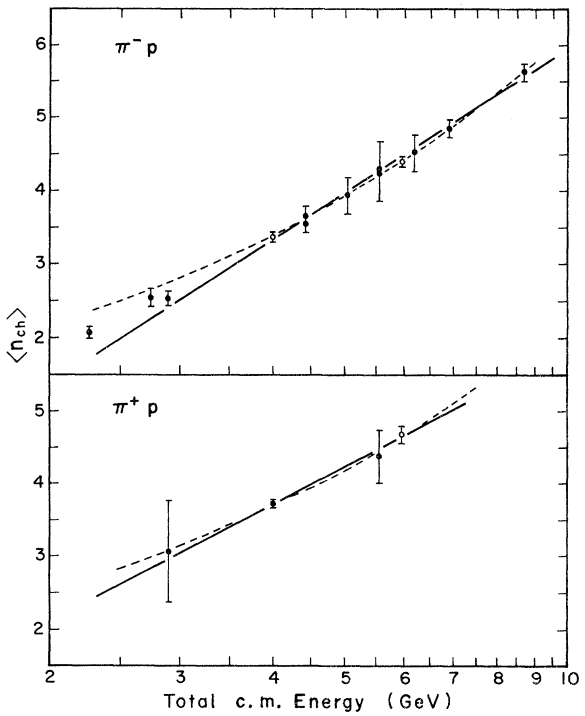

FIG. 4. Mean charged multiplicity $\langle n_{\rm ch}\rangle$ as a function of total c.m. energy for inelastic $\pi^{\pm}p$ interactions.

As has been pointed out by various authors,[13] there is a connection between multiplicity distributions and correlations among outgoing secondaries through integrals over the single- and two-particle distribution functions, $f(\vec{p}, s)$ and $g(\vec{p}_1, \vec{p}_2, s)$. A parameter of interest because there are definite predictions for its dependence on s is the quantity f_2 defined as

TABLE II. Multiplicity moments for inelastic πp interactions.

Multiplicity moments	8.05-GeV/c $\pi^- p$	18.5-GeV/c $\pi^- p$	18.5-GeV/c $\pi^+ p$
$\langle n_{\rm ch}\rangle$	3.37 ± 0.06	4.39 ± 0.04	4.68 ± 0.09
$\langle n_{\rm ch}^2\rangle$	13.69 ± 0.30	23.00 ± 0.31	25.19 ± 0.72
$\langle n_{\rm ch}^3\rangle$	62.92 ± 1.65	136.8 ± 2.1	152.0 ± 4.9
$\langle n_{\rm ch}(n_{\rm ch}-1)\rangle$	10.32 ± 0.25	18.61 ± 0.27	20.50 ± 0.63
$\langle n_{\rm ch}(n_{\rm ch}-1)(n_{\rm ch}-2)\rangle$	28.58 ± 0.88	76.6 ± 1.3	85.8 ± 3.0
$\langle n_-\rangle$	1.68 ± 0.03	2.20 ± 0.02	1.34 ± 0.05
$\langle n_-^2\rangle$	3.42 ± 0.07	5.75 ± 0.08	2.61 ± 0.09
$\langle n_-^3\rangle$	7.87 ± 0.21	17.10 ± 0.27	6.13 ± 0.21
$\langle n_-(n_- - 1)\rangle$	1.74 ± 0.05	3.55 ± 0.06	1.27 ± 0.04
$\langle n_-(n_- - 1)(n_- - 2)\rangle$	0.96 ± 0.04	4.24 ± 0.08	0.96 ± 0.04
$\langle n_+\rangle$	1.68 ± 0.03	2.20 ± 0.02	3.34 ± 0.05
$\langle n_+^2\rangle$	3.42 ± 0.07	5.75 ± 0.08	11.98 ± 0.27
$\langle n_+^3\rangle$	7.87 ± 0.21	17.10 ± 0.27	45.9 ± 1.3
$\langle n_+(n_+ - 1)\rangle$	1.74 ± 0.05	3.55 ± 0.06	8.64 ± 0.23
$\langle n_+(n_+ - 1)(n_+ - 2)\rangle$	0.96 ± 0.04	4.24 ± 0.08	16.65 ± 0.57

TABLE III. Energy dependence of $\langle n_{\rm ch}\rangle$.

Reaction	$\langle n_{\rm ch}\rangle$	A	B	χ^2	Degrees of freedom
$\pi^- p$ [a]	$A(E^{\rm c.m.})^B$	1.36 ± 0.12	0.66 ± 0.05	0.1	6
	$A + B \ln E_{\rm c.m.}$	−0.67 ± 0.36	2.87 ± 0.20	0.9	6
$\pi^+ p$ [b]	$A(E^{\rm c.m.})^B$	1.70 ± 0.28	0.56 ± 0.11	0.08	1
	$A + B \ln E_{\rm c.m.}$	0.47 ± 0.72	2.34 ± 0.51	0.11	1
pp [c]	$A(E^{\rm c.m.})^B$	1.49	0.56	14	7
	$A + B \ln E_{\rm c.m.}$	−0.88	2.76	8.9	6

[a] Expressions were fitted over the incident momentum range $8 \leq P_{\rm lab}^{\rm in} \leq 40$ GeV/c.

[b] Expressions were fitted over the incident momentum range $8 \leq P_{\rm lab}^{\rm in} \leq 18.5$ GeV/c.

[c] The power-law form was fitted over the incident momentum range $12 \leq P_{\rm lab}^{\rm in} \leq 200$ GeV/c, while the $\ln E^{\rm c.m.}$ fits extended only over the $12 \leq P_{\rm lab}^{\rm in} \leq 30$ GeV/c.

$$f_2 = \langle n(n-1)\rangle - \langle n\rangle^2 .$$

For a pure Poisson distribution $f_2 = 0$, while $f_2 < 0$ or $f_2 > 0$ if the distribution is narrower or broader than Poisson. The dependence of f_2 on s varies with different models. Fragmentation models imply an asymptotic behavior $f_2 \to +cs^{1/2}$. On the other hand, an independent-particle-emission view, or multiperipheral configuration with single emission of pions along a chain, predicts asymptotic distributions narrower than Poisson ($f_2 < 0$). Several authors[18] have tested this behavior, in pp and πp interactions. They all show the common feature that $f_2^{\rm ch}$ is negative at very low energies (<20 GeV/c) and becomes positive at ~50 GeV/c. We show in Fig. 5 values of $f_2/\langle n\rangle^2$ in terms of the charged multiplicity ($n = n_{\rm ch}$) and of the negative particle multiplicity ($n = n_-$) as a function of $s^{1/2}$. The observed behavior is similar to that seen by Berger, *et al.*[18] in pp interactions. For low energies $f_2^{\rm ch}/\langle n_{\rm ch}\rangle^2$ for πp interactions is negative, becoming positive at ~40 GeV/c. For multiplicities for negative particles, $f_2^-/\langle n_-\rangle^2$ is consistently negative even at 40 GeV/c.

In Table V, we present values of additional parameters which are of interest in the study of inelastic $\pi^- p$ interactions at 8.05 and 18.5 GeV/c and $\pi^+ p$ interactions at 18.5 GeV/c. These parameters have been calculated in terms of $n_{\rm ch}$, n_-, n_-^R, and n_-^L. The dispersion parameter D is defined by the expression

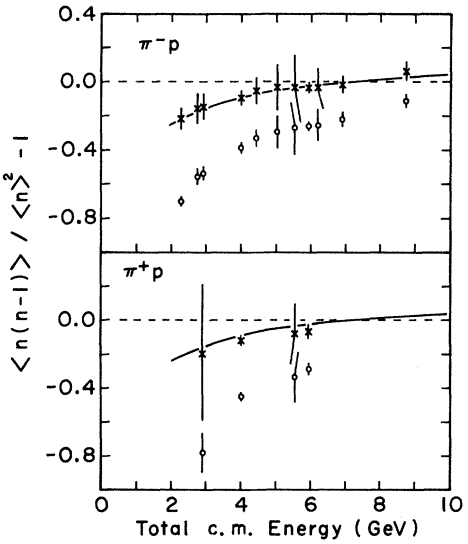

FIG. 5. Values of the quantity $(\langle n(n-1)\rangle/\langle n\rangle^2) - 1$ as a function of total c.m. energy for charged multiplicities, $n_{\rm ch}$(X), and negative particle multiplicities, n_-(○), in inelastic $\pi^{\pm}p$ interactions. The curves represent the expression $f_2^{\rm ch}/\langle n_{\rm ch}\rangle^2 = 0.2 - 0.74 s^{-1/3}$.

TABLE IV. Right and left multiplicity moments for inelastic $\pi^{\pm}p$ interactions.

Multiplicity moments	8.05-GeV/c π^-p	18.5-GeV/c π^-p	18.5-GeV/c π^+p
$\langle n_-^R\rangle$	1.10 ± 0.05	1.42 ± 0.06	0.795 ± 0.042
$\langle (n_-^R)^2\rangle$	1.69 ± 0.06	2.70 ± 0.08	1.21 ± 0.05
$\langle (n_-^R)^3\rangle$	3.04 ± 0.08	6.02 ± 0.12	2.20 ± 0.06
$\langle n_-^R(n_-^R-1)\rangle$	0.597 ± 0.026	1.28 ± 0.05	0.413 ± 0.022
$\langle n_-^R(n_-^R-1)(n_-^R-2)\rangle$	0.150 ± 0.008	0.757 ± 0.029	0.162 ± 0.009
$\langle n_-^L\rangle$	0.588 ± 0.025	0.767 ± 0.028	0.541 ± 0.029
$\langle (n_-^L)^2\rangle$	0.831 ± 0.028	1.25 ± 0.03	0.774 ± 0.031
$\langle (n_-^L)^3\rangle$	1.39 ± 0.04	2.50 ± 0.05	1.33 ± 0.04
$\langle n_-^L(n_-^L-1)\rangle$	0.243 ± 0.012	0.483 ± 0.018	0.233 ± 0.012
$\langle n_-^L(n_-^L-1)(n_-^L-2)\rangle$	0.0752 ± 0.0050	0.283 ± 0.013	0.0890 ± 0.0052
$\langle n_-^L n_-^R\rangle$	0.449 ± 0.020	0.886 ± 0.033	0.311 ± 0.017
$\langle n_-^L(n_-^L-1)n_-^R\rangle$	0.109 ± 0.007	0.454 ± 0.018	0.104 ± 0.006
$\langle n_-^R(n_-^R-1)n_-^L\rangle$	0.137 ± 0.008	0.602 ± 0.023	0.131 ± 0.007
$\langle (n_-^L)^2 n_-^R\rangle$	0.558 ± 0.021	1.34 ± 0.04	0.415 ± 0.018
$\langle (n_-^R)^2 n_-^L\rangle$	0.586 ± 0.022	1.49 ± 0.04	0.442 ± 0.018

$$D^2 = \langle n^2\rangle - \langle n\rangle^2 .$$

Our results are consistent with Wroblewski's observation that $D_{\rm ch}^2/\langle n_{\rm ch}\rangle^2$ is independent of s.

C. Mean Transverse Momentum

Finally, we consider the properties of the transverse momenta of secondaries in high-energy collisions. It is usually stated that the average transverse momentum $\langle P_T\rangle$ is small and relatively constant with increasing energy. However, cosmic-ray studies suggest[19] that there may be a slow rise of $\langle P_T\rangle$ from about 0.33 GeV/c at $s^{1/2} = 10$ GeV to about 0.50 GeV/c at $s^{1/2} = 10^5$ GeV.

Calculated values of $\langle P_T\rangle$ and $\langle P_T^2\rangle$ for our samples of negative pions from $\pi^- p$ interactions at 8.05 and 18.5 GeV/c and $\pi^+ p$ interactions at 18.5

TABLE V. Multiplicity parameters D^2 and f_2 for inelastic $\pi^{\pm}p$ interactions.

Parameter	8.05-GeV/c π^-p	18.5-GeV/c π^-p	18.5-GeV/c π^+p
$D_{\rm ch}^2$	2.34 ± 0.37	3.71 ± 0.31	3.28 ± 0.68
D_-^2	0.59 ± 0.09	0.93 ± 0.08	0.82 ± 0.04
$(D_-^L)^2$	0.48 ± 0.04	0.66 ± 0.05	0.48 ± 0.04
$(D_-^R)^2$	0.49 ± 0.13	0.68 ± 0.18	0.58 ± 0.08
$D_{\rm ch}^2/\langle n_{\rm ch}\rangle^2$	0.21 ± 0.04	0.19 ± 0.02	0.15 ± 0.04
$D_-^2/\langle n_-\rangle^2$	0.21 ± 0.04	0.19 ± 0.02	0.45 ± 0.05
$(D_-^L)^2/\langle n_-^L\rangle^2$	1.40 ± 0.22	1.13 ± 0.16	1.65 ± 0.30
$(D_-^R)^2/\langle n_-^R\rangle^2$	0.40 ± 0.14	0.34 ± 0.12	0.92 ± 0.22
$f_2^{\rm ch}$	−1.03 ± 0.40	−0.68 ± 0.34	−1.40 ± 0.75
f_2^-	−1.10 ± 0.11	−1.27 ± 0.09	−0.52 ± 0.08
f_2^L	−0.10 ± 0.03	−0.10 ± 0.05	−0.06 ± 0.03
f_2^R	−0.61 ± 0.12	−0.75 ± 0.17	−0.22 ± 0.07
$f_2^{\rm ch}/\langle n_{\rm ch}\rangle^2$	−0.09 ± 0.03	−0.04 ± 0.02	−0.06 ± 0.03
$f_2^-/\langle n_-\rangle^2$	−0.39 ± 0.02	−0.26 ± 0.01	−0.29 ± 0.02
$f_2^L/\langle n_-^L\rangle^2$	−0.30 ± 0.07	−0.18 ± 0.07	−0.20 ± 0.09
$f_2^R/\langle n_-^R\rangle^2$	−0.51 ± 0.05	−0.36 ± 0.06	−0.35 ± 0.08

GeV/c are shown in Table VI. A comparison of the values of $\langle P_T^2 \rangle$ for $\pi^- p$ interactions at 8.05 and 18.5 GeV/c seems to indicate a slightly higher value at 18.5 GeV/c. Both $\langle P_T \rangle$ and $\langle P_T^2 \rangle$ for 18.5 GeV/c $\pi^+ p$ interactions are lower than the $\pi^- p$ values. Values of $\langle P_T \rangle$ and $\langle P_T^2 \rangle$ are also given for different charge multiplicities. For a fixed energy, the mean transverse momentum decreases as the multiplicity increases. It has been suggested that this is purely a phase-space effect which reflects a decrease in the average energy of secondaries as the multiplicity grows.

V. SINGLE-PARTICLE INCLUSIVE REACTIONS

In this section we present an analysis of the production of a single negative pion in the reactions

$$\pi^- + p \to \pi^- + \text{anything} \quad (1)$$

at incident momenta of 8.05 and 18.5 GeV/c, and

$$\pi^+ + p \to \pi^- + \text{anything} \quad (2)$$

at an incident momentum of 18.5 GeV/c. By simultaneously studying data for reaction (1) at two different energies, we can discuss some of the tests for scaling in this energy range. By comparing reactions (1) and (2) at the same energy, we can observe the effects of the incident charge in pion-induced reactions. In the following sections, we will discuss first the hypothesis of limiting fragmentation in terms of finite momenta in the laboratory frame (proton fragmentation), and then distributions in terms of c.m. variables in order to determine the most useful set with which to study scaling, especially in the central region. Distributions are presented in terms of x and P_T^2, y, and P_T^2, and y_r and P_T^2.

TABLE VI. Mean transverse momentum.

	Number of charged secondaries	8.05-GeV/c $\pi^- p$	18.5-GeV/c $\pi^- p$	18.5-GeV/c $\pi^+ p$
$\langle P_T \rangle$ (GeV/c)	all	0.341 ± 0.002	0.342 ± 0.001	0.311 ± 0.001
	2	0.375 ± 0.003	0.361 ± 0.002	···
	4	0.341 ± 0.002	0.356 ± 0.001	0.331 ± 0.001
	6	0.300 ± 0.003	0.336 ± 0.001	0.312 ± 0.001
	8	0.250 ± 0.008	0.307 ± 0.002	0.289 ± 0.001
	10	0.178 ± 0.034	0.270 ± 0.003	0.258 ± 0.002
	12	···	0.233 ± 0.008	0.228 ± 0.006
	14	···	0.208 ± 0.023	0.192 ± 0.011
$\langle P_T^2 \rangle$ [(GeV/c)^2]	all	0.159 ± 0.002	0.170 ± 0.001	0.140 ± 0.001
	2	0.183 ± 0.003	0.187 ± 0.002	···
	4	0.160 ± 0.002	0.185 ± 0.002	0.159 ± 0.001
	6	0.128 ± 0.003	0.163 ± 0.001	0.140 ± 0.001
	8	0.082 ± 0.005	0.137 ± 0.002	0.120 ± 0.001
	10	0.043 ± 0.018	0.104 ± 0.003	0.096 ± 0.002
	12	···	0.078 ± 0.006	0.074 ± 0.004
	14	···	0.070 ± 0.015	0.046 ± 0.005

A. Finite Laboratory Momenta and Limiting Target Fragmentation

We first consider the hypothesis of limiting fragmentation proposed by Benecke, *et al.*[20] which suggests that the spectra of particles with finite momenta in the laboratory, that is, fragments of the proton, should be independent of the total c.m. energy $s^{1/2}$ as $s^{1/2}$ becomes large. In order to test this hypothesis we present in Fig. 6(a) the structure function $H_1(P_l)$ as a function of P_l for reactions (1) and (2), where

$$H_1(P_l) = \int_{\text{all } P_T^2} f(P_l, P_T^2) dP_T^2$$

and the Lorentz-invariant differential cross section is given by

$$f(P_l, P_T^2) = \frac{E}{\pi} \frac{d\sigma}{dP_l dP_T^2} .$$

We note that for reaction (1), $H_1(P_l)$ for the 18.5-GeV/c data are systematically lower than at 8.05 GeV/c, for $P_l \lesssim 0.4$ GeV/c. For P_l between 0.4 and 1.7 GeV/c, the two distributions are nearly identical. The drop in the 8.05-GeV/c distribution

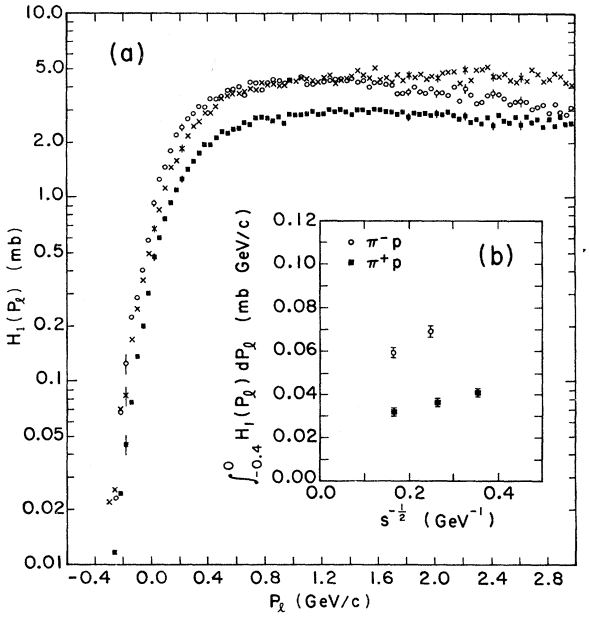

FIG. 6. (a) Distributions of the structure function $H_1(P_l) = \int f(P_l, P_T) dP_T^2$ as a function of P_l for the reactions $\pi^- + p \to \pi^- +$ anything at 8.05 GeV/c (○) and 18.5 GeV/c (×) and $\pi^+ + p \to \pi^- +$ anything at 18.5 GeV/c (■). (b) Values of the integral $\int_{-0.4}^{0} H_1(P_l) dP_l$ as a function of $s^{-1/2}$ for the reactions $\pi^- + p \to \pi^- +$ anything at 8.05 and 18.5 GeV/c and $\pi^+ p \to \pi^- +$ anything at 3.7, 7.0, and 18.5 GeV/c. The values at 3.7 and 7.0 GeV/c are taken from Ref. 4.

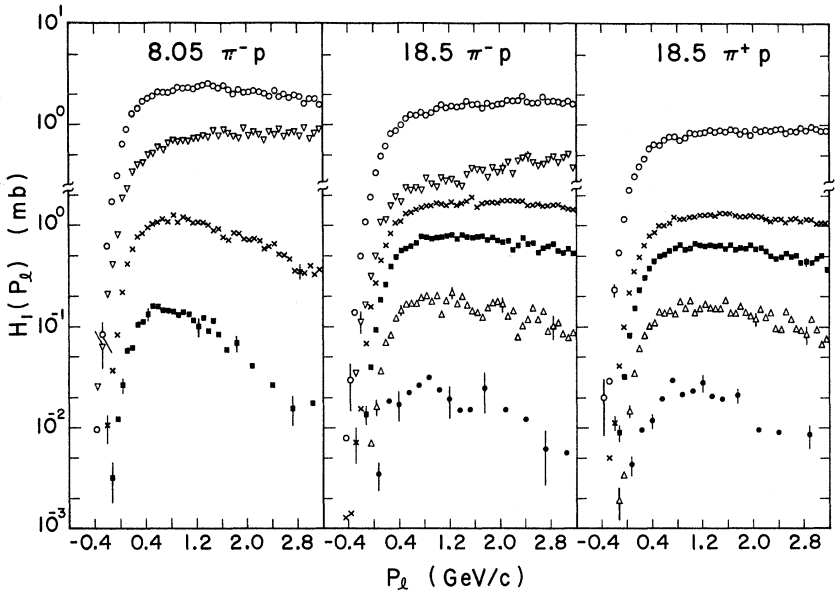

FIG. 7. Distributions of the structure function $H_1(P_l)$ as a function of P_l for the various charge multiplicities n, in the reactions $\pi^- + p \to \pi^- +$ anything at 8.05 and 18.5 GeV/c and $\pi^+ + p \to \pi^- +$ anything at 18.5 GeV/c. Distributions are shown for $n = 2$ (▽), $n = 4$ (○), $n = 6$ (×), $n = 8$ (■), $n = 10$ (△), and $n = 12$ (●). Refer to the left-hand scale opposite the highest point on each curve.

for $P_l > 1.7$ GeV/c is a result of the different kinematic limits of P_l at the two energies. Comparing reactions (1) and (2) at 18.5 GeV/c, we note that reaction (2) is about 30–40% lower, but essentially the same shape over most of the range of P_l shown. For $P_l < 0$, however, the cross section for reaction (2) drops off faster than that for reaction (1).

In Fig. 7, we have plotted $H_1(P_l)$ as a function of P_l for different charge multiplicities, n. In the region $P_l < 0$, we observe that the distributions decrease more rapidly as the multiplicity increases. The rate of decrease for 2-prongs and 4-prongs in reaction (1) is about the same for 8.05 and 18.5 GeV/c. However, the contribution of low-multiplicity events ($n \leq 4$) in this region is ~83% at 8.05 GeV/c and ~57% at 18.5 GeV/c. Thus, the fact that the cross section at 8.05 GeV/c is higher in this region for the over-all distribution [Fig. 6(a)] can be mostly attributed to a higher contribution from low-multiplicity events.

By studying only pions produced backward ($P_l < 0$) in the laboratory, we restrict our study to a kinematic region where the momenta remain finite as $s \to \infty$ and refer to these particles as target fragments. The fact that the distributions in the region are not identical [see Fig. 6(a)] indicates that the limiting-fragmentation hypothesis is not exactly satisfied for proton fragmentation in reaction (1) in this energy range. The energy dependence may also be seen in Fig. 8 where we show the structure function $H_2(P_T^2)$ as a function of P_T^2, where

$$H_2(P_T^2) = \int_{\text{all } P_l < 0} f(P_l, P_T^2) dP_l .$$

Again the 8.05-GeV/c points lie above the 18.5-GeV/c points, except in the low P_T^2 region [$P_T^2 < 0.05$ (GeV/c)^2]. In both Figs. 6(a) and 8 the points for reaction (2) at 18.5 GeV/c lie significantly be-

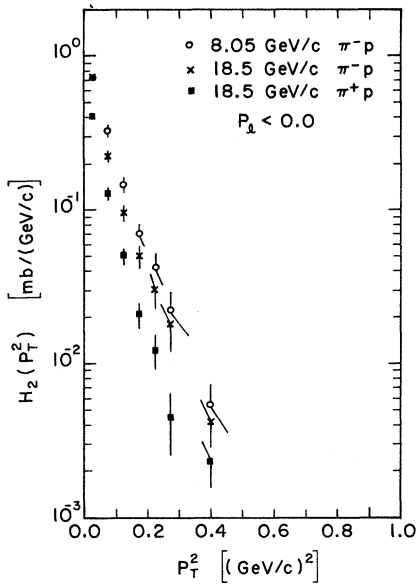

FIG. 8. Distributions of the structure function $H_2(P_T^2) = \int_{-0.4}^{0} f(P_l, P_T^2) dP_l$ as a function of P_T^2 for the three sets of data of Fig. 6(a).

low those for reaction (1) at 18.5 GeV/c. In Fig. 9, we show the dependence of the proton fragmentation cross section on P_l and P_T^2 in more detail. Here we plot $f(P_l, P_T^2)$ as a function of P_l averaged over various P_T^2 intervals. The deviations from limiting fragmentation illustrated in Figs. 6(a) and 8 are seen here as differences in the invariant differential cross sections.

We have integrated $H_1(P_l)$ over all $P_l < 0$ for reactions (1) and (2) and have plotted the values as a function of $s^{-1/2}$ in Fig. 6(b). For reaction (2), we show values of these integrals from published data[4] at 3.7 and 7.0 GeV/c, in addition to our data. As $s^{-1/2} \to 0$ we observe a rapid fall in the cross section for the reaction $\pi^- p \to \pi^-$. On the other hand, the cross section for the reaction $\pi^+ p \to \pi^-$, shows a much weaker dependence on s. The differences in the s dependence of the cross section for these reactions are consistent with the predictions of Chan *et al.*[21] In both reactions the cross section variation with s is consistent with the form $A + Bs^{-1/2}$.

B. Distributions in Terms of x and P_T^2

We present here distributions for reactions (1) and (2) in terms of the Feynman x variable and P_T^2 as defined in Sec. I. The range of x is $-1 < x < +1$ independent of the incident momentum. Negative values of x refer to pions produced with longitudinal momenta in the direction of the incident proton in the c.m. system and positive values refer to pions with longitudinal momenta in the direction of the incident pion. The invariant cross section is given by

$$f(x, P_T^2) = \frac{E^{\text{c.m.}}}{\pi P_0^{\text{c.m.}}} \frac{d\sigma}{dx dP_T^2} .$$

In Fig. 10 we show distributions of the structure function

$$F_1(x) = \int_{\text{all } P_T^2} f(x, P_T^2) dP_T^2$$

as a function of x for reaction (1) at 8.05 and 18.5 GeV/c and reaction (2) at 18.5 GeV/c. In contrast to reactions such as $pp \to \pi$ + anything we clearly see effects due to the differences between the incident particles. It has been observed[22] that, in many events one of the incident particles is quasi-elastically scattered and carries off a sizable fraction of the energy. This is referred to as a leading particle. For reaction (1) one of the incident particles is identical to the inclusive particle under study and, thus, leading-particle effects may be important. We observe an asymmetry about $x = 0$ in distributions of $F_1(x)$ for both reactions (1) and (2). More pions are produced with

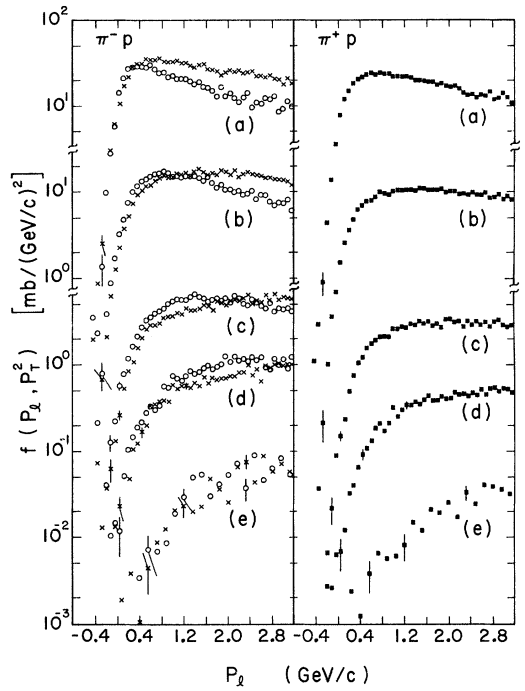

FIG. 9. Distributions of the invariant cross section $f(P_l, P_T^2)$ as a function of P_l for the three sets of data of Fig. 6(a), averaged over the P_T^2 intervals: (a) $0.0 < P_T^2 < 0.04$, (b) $0.04 < P_T^2 < 0.16$, (c) $0.16 < P_T^2 < 0.36$, (d) $0.36 < P_T^2 < 1.0$, and (e) $1.0 < P_T^2 < 2.0$. All P_T^2 intervals are given in (GeV/c)^2. Data for $\pi^- + p \to \pi^-$ + anything at 8.05 and 18.5 GeV/c are shown as (○) and (X), respectively; data for $\pi^+ + p \to \pi^+$ + anything at 18.5 GeV/c are shown as (■).

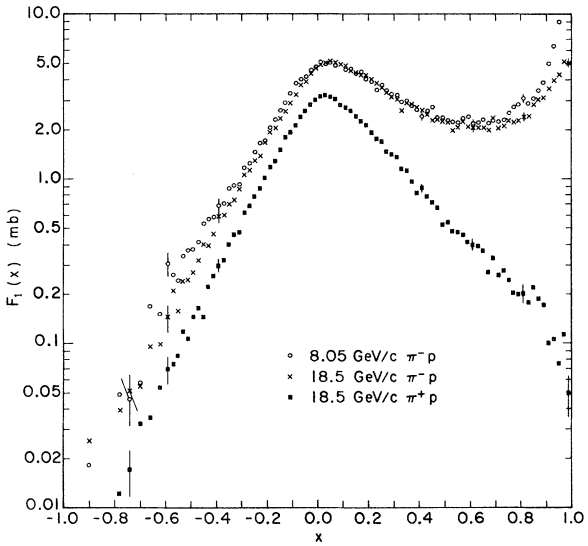

FIG. 10. Distribution of the structure function $F_1(x) = \int f(x, P_T^2) dP_T^2$ as a function of x for the reactions $\pi^- + p \to \pi^-$ + anything at 8.05 and 18.5 GeV/c and $\pi^+ + p \to \pi^-$ + anything at 18.5 GeV/c.

$x>0$ than with $x<0$. The asymmetry for reaction (1) is understandable as a leading-particle effect. However, the existence of an asymmetry in $F_1(x)$ for reaction (2), where the incident particle is a π^+, would indicate that the asymmetry cannot be explained entirely as a leading-particle effect. We have examined separately the structure function $F_1(x)$ for different charge multiplicities in reactions (1) and (2). These distributions are shown in Fig. 11 and are observed to differ significantly for the various multiplicities. The distributions for higher multiplicity are more strongly peaked near $x=0$ than those for the low multiplicity events. For a fixed energy the asymmetry about $x=0$ decreases as the multiplicity grows. In reaction (1) the asymmetry for a fixed multiplicity increases between 8.05 and 18.5 GeV/c. We note that the large $|x|$ regions in the over-all distributions of $F_1(x)$ (Fig. 10) are dominated by low-multiplicity events.

We observe in Fig. 10 that there is little energy dependence in $F_1(x)$ for reaction (1) between 8.05 and 18.5 GeV/c over the range $-0.1<x<0.6$. For $x<-0.1$ the values of $F_1(x)$ for 8.05 GeV/c are consistently higher than the values at 18.5 GeV/c. This effect is equivalent to that observed in distributions of $H_1(P_t)$ for $P_t<0.4$ GeV/c [Fig. 6(a)]. The 8.05-GeV/c distribution is higher than the 18.5-GeV/c distribution for $x>0.6$ also. This region, near $x=+1$, is dominated by 2-prong events and includes elastic events where the π^- has close to the maximum allowed laboratory momentum. The elastic scattering cross section is decreasing from 8.05 to 18.5 GeV/c (see Table I). The poorer momentum resolution at 18.5 GeV/c also tends to reduce the apparent height of the forward peak. We note for comparison that the "unphysical" cross section for 2-prong events with measured π^- momenta corresponding to $x>+1$ for 18.5 GeV/c is 1.34 mb whereas it is 0.97 for 8.05 GeV/c.

Abarbanel[23] has suggested that $F_1(x)$ in the central region near $x=0$ might exhibit an energy dependence of the form $s^{-1/4}$. In order to compare our data with other published values, we have evaluated $F_1(x')$ averaged over the interval $-0.02<x'<0.02$, where $x'=2P_l^{\text{c.m.}}/s^{1/2}$ and

$$F_1(x')=\int_{\text{all } P_T^2} f(x', P_T^2)dP_T^2 .$$

The invariant cross section is then

$$f(x', P_T^2)=\frac{2E^{\text{c.m.}}}{\pi s^{1/2}}\frac{d\sigma}{dx'dP_T^2} .$$

In Fig. 12(a) we have plotted $F_1(x'=0)$ as a function of $s^{-1/4}$ for reaction (1) at 8.05 and 18.5 GeV/c and reaction (2) at 3.7, 7.0, and 18.5 GeV/c. (The values at 3.7 and 7.0 GeV/c are taken from Ref. 4.) The data are consistent with an $s^{-1/4}$ dependence, but other s dependence such as $s^{-1/2}$ cannot be ruled out. Reaction (1) exhibits very little energy dependence, while there is a rapid increase of $F_1(x'=0)$ with increasing energy for reaction (2). It is not at all surprising that reaction (2) is so strongly energy dependent since $\sigma(\pi^-)$, the total

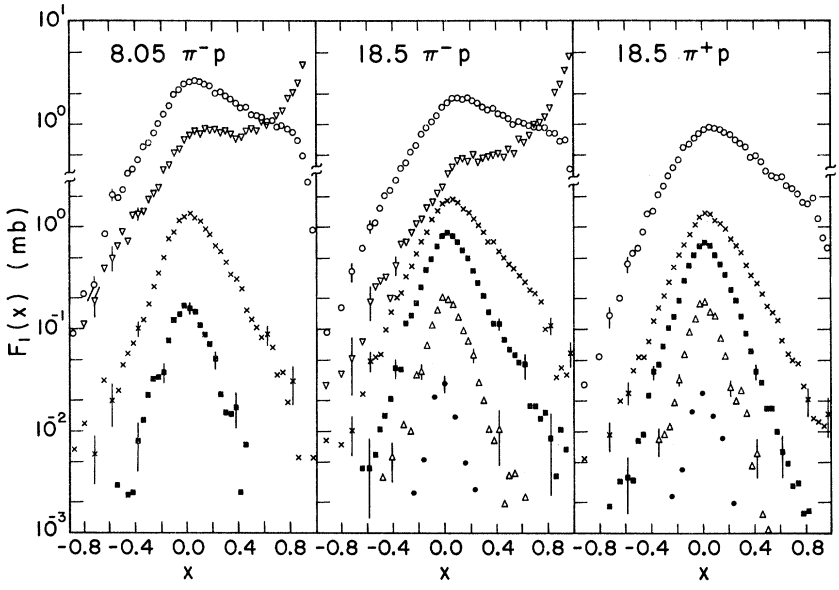

FIG. 11. Distributions of the structure function $F_1(x)$ as a function of x for the various charge multiplicities n for the three sets of data of Fig. 10. Distributions are shown for $n=2$ (▽), $n=4$ (○), $n=6$ (X), $n=8$ (■), $n=10$ (△), and $n=12$ (●). Refer to the left-hand scale opposite the highest point on each curve.

cross section for producing at least one π^- inelastically, is also rapidly rising from 3.7 to 18.5 GeV/c. We note that $\sigma(\pi^-)$ has values of 10.3, 12.8, and 16.6 mb at 3.7, 7.0, and 18.5 GeV/c, respectively. For reaction (1), on the other hand, $\sigma(\pi^-)$ shows little energy dependence between 8.05 and 18.5 GeV/c. Reaction (2) is obviously not developed in this sense. In Fig. 12(b) we show values of $F_1(x'=0)$ normalized by the total cross section for producing at least one π^- inelastically in reactions (1) and (2). We observe little variation with $s^{-1/4}$ for reaction (1), and much less energy dependence for the normalized $F_1(x'=0)$ for reaction (2) than for the unnormalized structure function in Fig. 12(a).

In Fig. 13(a) we have plotted the invariant differential cross section $f(x, P_T^2)$ as a function of x averaged over various P_T^2 intervals. The invariant cross sections for reaction (1) at 8.05 and 18.5 GeV/c are quite similar over a significant region of x near $x=0$ for all but the smallest and largest P_T^2 intervals. For $x<-0.1$ the 8.05-GeV/c distributions lie above the 18.5-GeV/c distributions for all but large values of P_T^2. For small P_T^2 the distribution is sharply peaked at $x=0$. As P_T^2 increases the peaks of the distributions move toward positive x and the distributions become broader. The equivalent distributions for reaction (2) at 18.5 GeV/c, Fig. 13(b), show the same change in shape for different P_T^2 intervals as reaction (1).

We now consider the features of the P_T^2 distributions for reactions (1) and (2). The structure function

$$F_2(P_T^2) = \int_{-1}^{+1} f(x, P_T^2)\,dx$$

is plotted as a function of P_T^2 in Fig. 14 for our three sets of data. The distributions are seen to be qualitatively similar, although significant differences are present. For reaction (1) $F_2(P_T^2)$ is significantly larger at 18.5 GeV/c for very small P_T^2, while the 18.5-GeV/c points lie below the

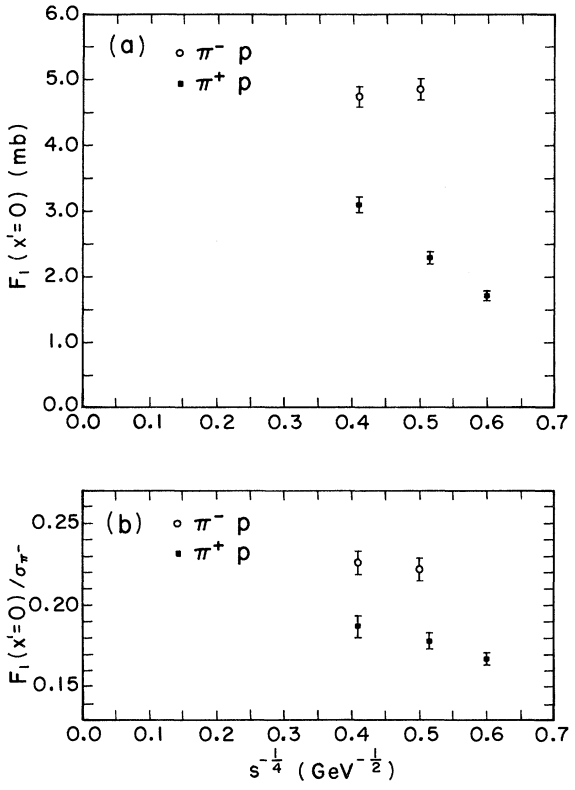

FIG. 12 (a) Values of the structure function $F_1(x')$ averaged over the interval $-0.02<x'<0.02$ as a function of $s^{-1/4}$ for the reactions $\pi^- + p \to \pi^-$ + anything at 8.05 and 18.5 GeV/c and $\pi^+ p \to \pi^-$ + anything at 3.7, 7.0, and 18.5 GeV/c. The values at 3.7 and 7.0 GeV/c are taken from Ref. 4. (b) Values of $F_1(x')$ normalized to the total cross section for producing at least one π^- inelastically. Values used for $\sigma(\pi^-)$ are: 22.0 and 20.8 mb for 8.05 and 18.5 GeV/c $\pi^- p$, respectively; 10.3, 12.8, and 16.6 mb for 3.7, 7.0, and 18.5 GeV/c $\pi^+ p$, respectively.

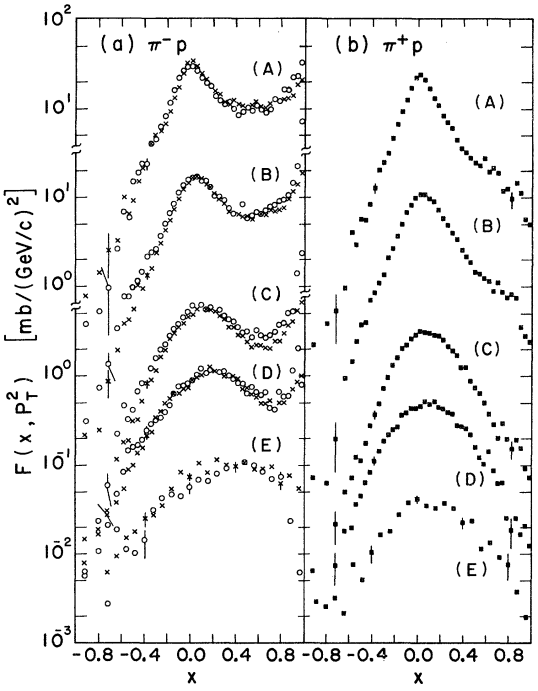

FIG. 13. (a) Distribution on the invariant cross section $f(x, P_T^2)$ as a function of x for the reaction $\pi^- p \to \pi^-$ + anything at 8.05 GeV/c (○) and 18.5 GeV/c (X), averaged over the P_T^2 intervals: (A) $0.0<P_T^2<0.04$, (B) $0.04<P_T^2<0.16$, (C) $0.16<P_T^2<0.36$, (D) $0.36<P_T^2<1.0$, and (E) $1.0<P_T^2<2.0$. All P_T^2 intervals are given in (GeV/c)^2. (b) Distributions of the invariant cross section $f(x, P_T^2)$ as a function of x for the reaction $\pi^+ + p \to \pi^-$ + anything at 18.5 GeV/c, averaged over the same P_T^2 intervals.

8.05-GeV/c data over the range $0.02 < P_T^2 < 0.40$ (GeV/c)^2. At large P_T^2 the 18.5-GeV/c distribution lies above the low-energy data although the difference is less significant. As P_T^2 increases the distribution for reaction (2) falls more rapidly than that for reaction (1) at 18.5 GeV/c. Distributions of $F_2(P_T^2)$ for the various charge multiplicities are shown in Fig. 15 for reactions (1) and (2). The distributions are more sharply peaked for the higher-multiplicity final states. We note that the major difference in the distribution of Fig. 14 for reaction (1) at 8.05 and 18.5 GeV/c appears to be due to the two-prong events.

C. Distributions in Terms of y and P_T^2

In Sec. II we discussed the usefulness of the rapidity variable y which permits the study of the region near $x = 0$ in more detail. We present here the inclusive reaction distributions in terms of y and P_T^2. In Fig. 16 we have plotted the structure function $G_1(y)$ as a function of y for reaction (1) at 8.05 and 18.5 GeV/c and reaction (2) at 18.5 GeV/c, where

$$G_1(y) = \int_{\text{all } P_T^2} f(y, P_T^2) dP_T^2 ,$$

with

$$f(y, P_T^2) = \frac{1}{\pi} \frac{d\sigma}{dy dP_T^2} .$$

We first note that the shapes of the distributions for $y < 0$ are generally similar. The kinematically allowed range from minimum to maximum rapidity in reaction (1) is 6.71 units of rapidity at 8.05 GeV/c and 7.46 units of rapidity at 18.5 GeV/c. The prominent elastic peaks observed in $F_1(x)$ at $x \approx +1$ for reaction (1) (see Fig. 10) appear in $G_1(y)$ as broad, rounded peaks, with maxima at different values of y for the two energies.

The distributions of $G_1(y)$ for reaction (1) show little energy dependence in the immediate vicinity

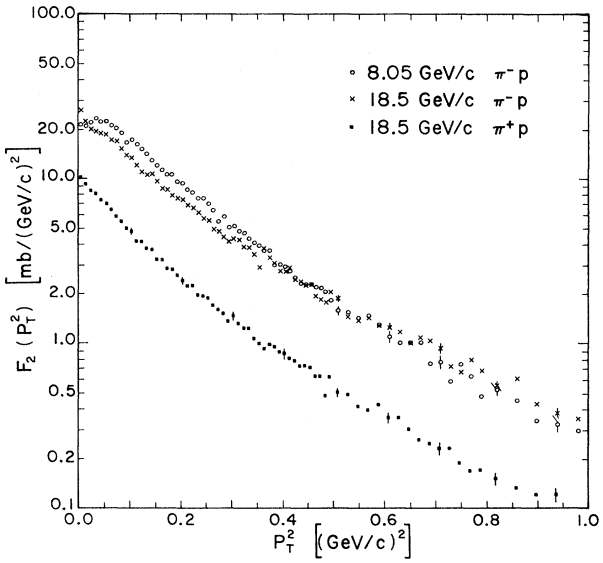

FIG. 14. Distributions of the structure function $F_2(P_T^2) = \int f(x, P_T^2) dx$ as a function of P_T^2 for the three sets of data of Fig. 10.

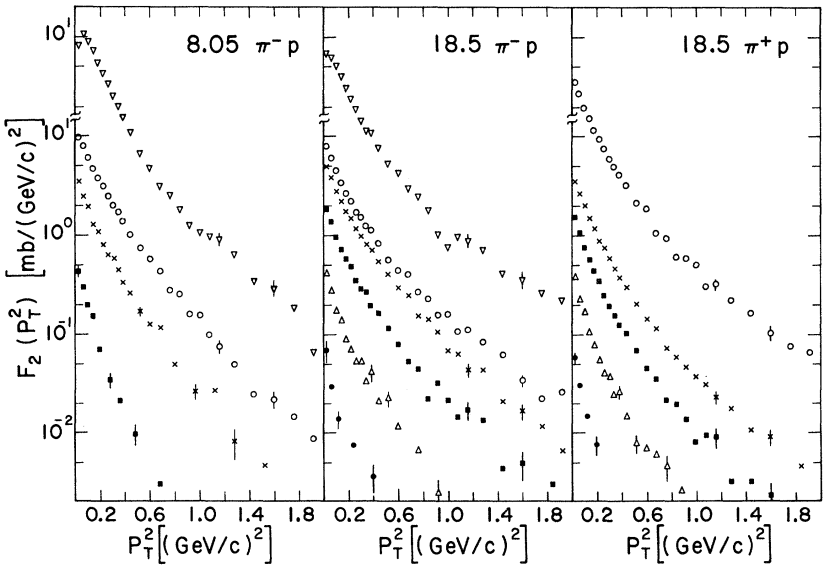

FIG. 15. Distributions of the structure function $F_2(P_T^2)$ as a function of P_T^2 for the various charge multiplicities n for the three sets of data of Fig. 10. Distributions are shown for $n = 2$ (▽), $n = 4$ (○), $n = 6$ (X), $n = 8$ (■), $n = 10$ (△), and $n = 12$ (●).

of $y=0$, e.g., for $|y| \lesssim 0.5$. For $|y|>0.5$, however, the distributions deviate significantly from one other. The differences are due, to a great extent, to kinematics, since the kinematically allowed region is a function of s as well as P_T^2 (see Sec. II). In order to show the P_T^2 dependence more clearly, we have plotted $f(y, P_T^2)$ as a function of y averaged over various P_T^2 intervals for reactions (1) and (2) in Fig. 17. As P_T^2 becomes larger, the widths of the distributions of $f(y, P_T^2)$ become narrower [recall Fig. 1(b)]. This effect is seen clearly for reaction (1) where we observe the shift of the elastic peak toward the center of the distribution as P_T^2 increases.

We have also studied the P_T^2 distributions for reactions (1) and (2) in terms of the structure function

$$G_2(P_T^2) = \int_{\text{all } y} f(y, P_T^2) dy .$$

Distributions of $G_2(P_T^2)$ as a function of P_T^2 are shown in Fig. 18. For reaction (1) the 18.5-GeV/c distribution lies consistently above the 8.05-GeV/c data over the whole range of P_T^2. The s-dependence is most apparent for $P_T^2 \lesssim 0.1$ (GeV/c)^2 and $P_T^2 \gtrsim 0.35$ (GeV/c)^2.

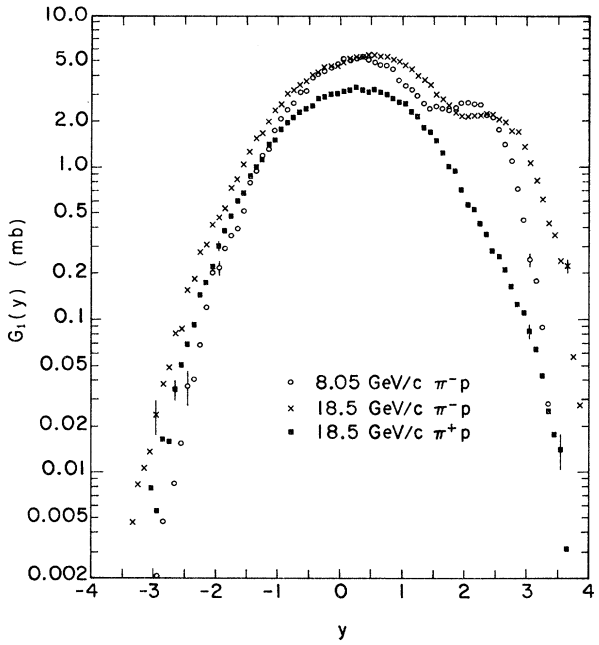

FIG. 16. Distribution of the structure function $G_1(y) = \int f(y, P_T^2) dP_T^2$ as a function of y for the reactions $\pi^- + p \to \pi^-$ + anything at 8.05 and 18.5 GeV/c and $\pi^+ p \to \pi^-$ + anything at 18.5 GeV/c.

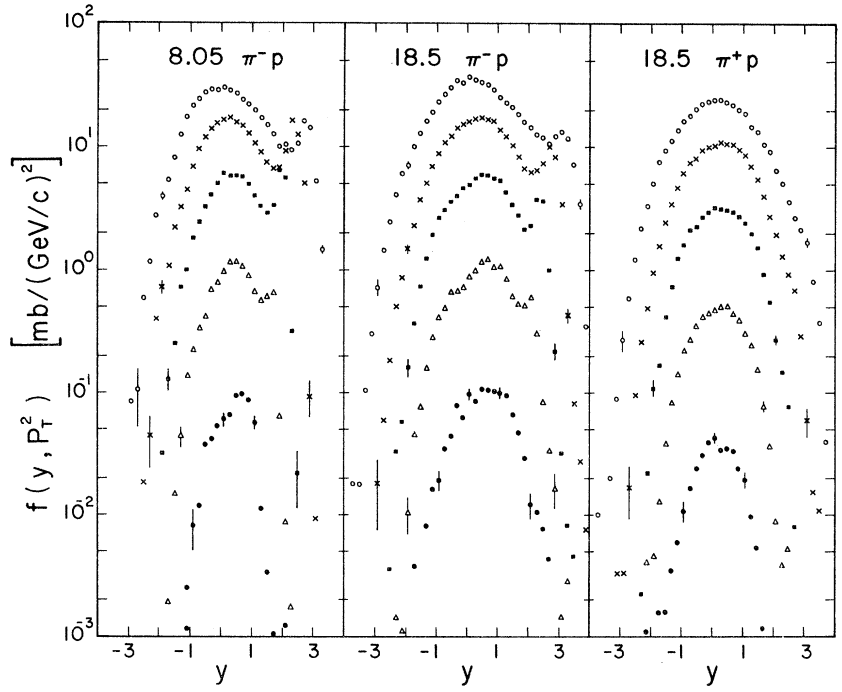

FIG. 17. Distributions of the invariant cross section $f(y, P_T^2)$ as a function of y for the three sets of data of Fig. 16, averaged over the P_T^2 intervals: $0.0 < P_T^2 < 0.04$ (○), $0.04 < P_T^2 < 0.16$ (X), $0.16 < P_T^2 < 0.36$ (■), $0.36 < P_T^2 < 1.0$ (△), and $1.0 < P_T^2 < 2.0$ (●). All P_T^2 intervals are given in (GeV/c)^2.

D. Distributions in Terms of y_r and P_T^2

We now display our data in terms of reduced rapidity y_r and P_T^2, as discussed in Sec. II. In Fig. 19 we show distributions of the structure function $R_1(y_r)$ as a function of y_r for reaction (1) at 8.05 and 18.5 GeV/c and reaction (2) at 18.5 GeV/c, where

$$R_1(y_r) = \int_{\text{all } P_T^2} f(y_r, P_T^2) dP_T^2$$

with the invariant cross section given by

$$f(y_r, P_T^2) = \frac{2}{\pi Y} \frac{d\sigma}{dy_r dP_T^2} .$$

Using this reduced form of the rapidity variable, which has a range of $-1 < y_r < +1$, we note that the leading-particle effects which were smeared out in distributions of y are now clearly discernible for reaction (1) at the two energies. The distributions of $R_1(y_r)$, however, expand the region near $x = 0$, thus retaining this property of the rapidity y. The shapes of the distributions for reaction (1) and reaction (2) are very similar for $y_r < 0$. For reaction (1), only small differences in the distributions for 8.05 and 18.5 GeV/c are observed. In order to study this behavior in more detail, we show in Fig. 20(a) distributions of $f(y_r, P_T^2)$ as a function of y_r averaged over various P_T^2 intervals. Distributions for reaction (1) at 8.05 and 18.5 GeV/c have been plotted together so that similarities will be evident. We find that the invariant cross sections over a wide range of the central region are the same at both energies for all but the smallest and largest

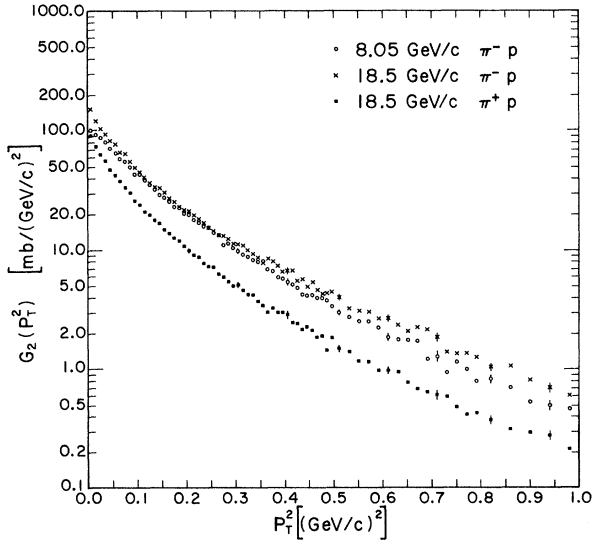

FIG. 18. Distributions of the structure function $G_2(P_T^2) = \int f(y, P_T^2) dy$ as a function of P_T^2 for the three sets of data of Fig. 16.

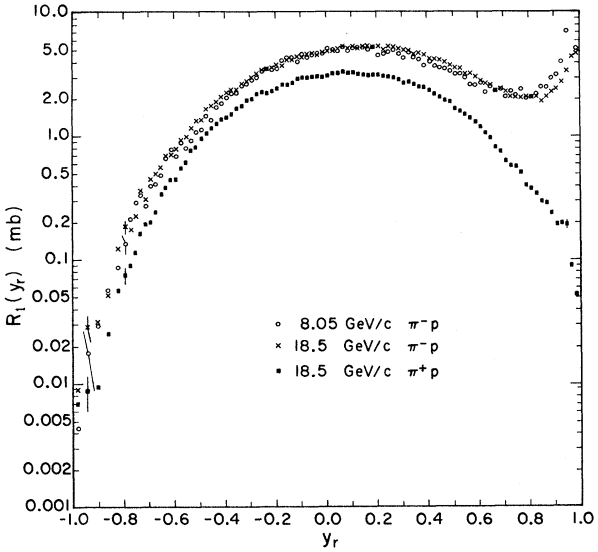

FIG. 19 Distributions of the structure function $R_1(y_r) = \int f(y_r, P_T^2) dP_T^2$ as a function of y_r for the reactions $\pi^- + p \to \pi^- +$ anything at 8.05 and 18.5 GeV/c and $\pi^+ + p \to \pi^- +$ anything at 18.5 GeV/c.

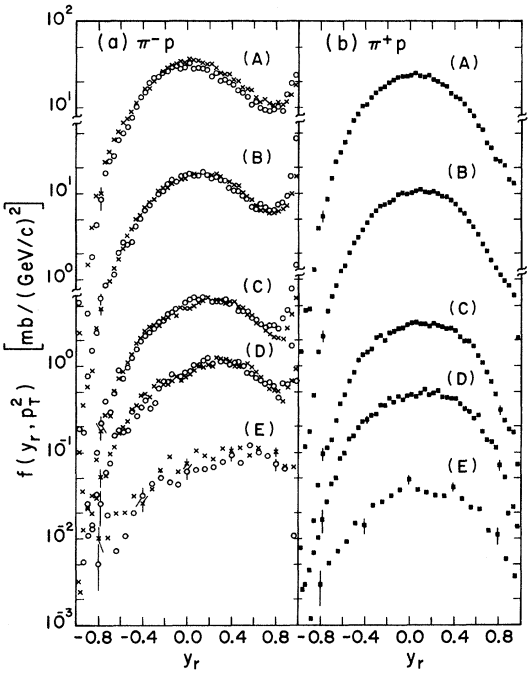

FIG. 20. (a) Distributions of the invariant cross section $f(y_r, P_T^2)$ as a function of y_r for the reactions $\pi^- + p \to \pi^- +$ anything at 8.05 GeV/c (○) and 18.5 GeV/c (×), averaged over the P_T^2 intervals: (A) $0.0 < P_T^2 < 0.04$, (B) $0.04 < P_T^2 < 0.16$, (C) $0.16 < P_T^2 < 0.36$, (D) $0.36 < P_T^2 < 1.0$, (E) $1.0 < P_T^2 < 2.0$. All P_T^2 intervals are given in $(\text{GeV}/c)^2$. (b) Distributions of the invariant cross section $f(y_r, P_T^2)$ as a function of y_r for the reaction $\pi^+ + p \to \pi^- +$ anything at 18.5 GeV/c, averaged over the same P_T^2 intervals.

intervals of P_T^2. We have also plotted, in Fig. 20(b), corresponding distributions of $f(y_r, P_T^2)$ for reaction (2) at 18.5 GeV/c. We observe very little change in the shapes of the distributions as P_T^2 is varied, especially in the central region. This is to be contrasted with the striking changes in shape for distributions of $f(x, P_T^2)$ as a function x (Fig. 13) and $f(y, P_T^2)$ as a function of y (Fig. 17) averaged over various P_T^2 regions.

We have also studied the P_T^2 distributions for reactions (1) and (2) in terms of the structure function

$$R_2(P_T^2) = \int_{-1}^{+1} f(y_r, P_T^2) dy_r \ ,$$

shown as a function of P_T^2 in Fig. 21. We observe that the $R_2(P_T^2)$ distributions for reaction (1) at the two incident momenta differ significantly only for $P_T^2 < 0.02$ (GeV/c)^2. The distribution for reaction (2) decreases more rapidly as P_T^2 is increased than the distributions for reaction (1).

In Fig. 22 we show distributions of $f(y_r, P_T^2)$ as a function of P_T^2 averaged over various positive and negative y_r intervals for reactions (1) and (2). For reaction (1) we observe excellent agreement between the invariant cross sections at the two energies throughout the entire region of y_r except for $y_r > +0.6$. We note, however, disagreement for $P_T^2 < 0.04$ (GeV/c)^2, where the 18.5-GeV/c points are consistently higher. The distributions of $f(y_r, P_T^2)$ for reaction (2) have essentially the same shape except for deviations at small P_T^2 when $y_r > +0.2$. To emphasize the similarity, we have plotted curves of the form $A \exp[-(P_T^2 + m_\pi^2/T)^{1/2}]$ normalized to the data of reaction (2) for each y_r interval with $T = 0.15$ GeV/c. It is interesting that this parametrization gives a rather good fit to the data at all but the largest $|y_r|$ intervals, and even here it fails only for small P_T^2.

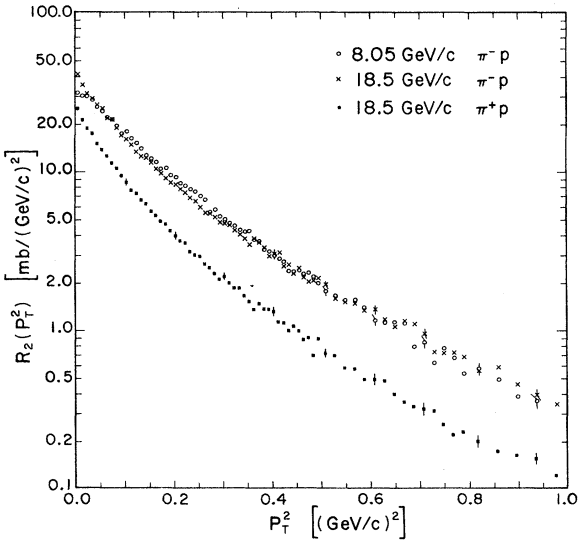

FIG. 21. Distributions of the structure function $R_2(P_T^2) = \int f(y_r, P_T^2) dy_r$ as a function of P_T^2 for the three sets of data of Fig. 19.

VI. DISCUSSION

In the previous sections we have presented our data in terms of several sets of c.m. variables. Motivated by predictions of scaling in inclusive reactions, we have attempted to determine the set of variables for which the distributions of the structure functions exhibit the least energy dependence. It is interesting to compare the ratios of the various structure functions for reaction (1) at 8.05 and 18.5 GeV/c.

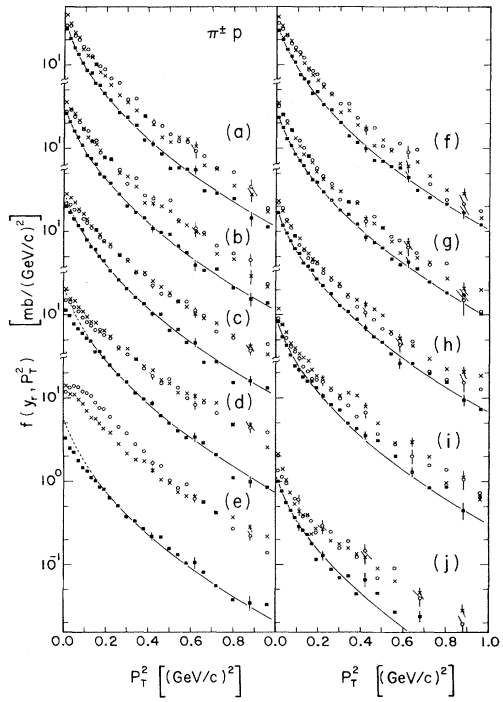

FIG. 22. Distributions of the invariant cross section $f(y_r, P_T^2)$ as a function of P_T^2 for the three sets of data of Figs. 19, 20, and 21 averaged over the positive y_r intervals: (a) $0.0 < y_r < 0.1$, (b) $0.1 < y_r < 0.2$, (c) $0.2 < y_r < 0.4$, (d) $0.4 < y_r < 0.6$, (e) $0.6 < y_r < 1.0$, and the negative y_r intervals: (f) $-0.1 < y_r < 0.0$, (g) $-0.2 < y_r < -0.1$, (h) $-0.4 < y_r < -0.2$, (i) $-0.6 < y_r < -0.4$, and (j) $-1.0 < y_r < -0.6$. The solid curves represent the expression $f(y_r, P_T^2) = C[\exp(-\mu/T]$ normalized to each distribution separately, where $\mu = (P_T^2 + m_\pi^2)^{1/2}$ and $T = 150$ MeV. The dashed curves show regions of P_T^2 which were not consistent with this functional form. Data for the reactions $\pi^- + p \to \pi^- +$ anything at 8.05 and 18.5 GeV/c and $\pi^+ p \to \pi^- +$ anything at 18.5 GeV/c are shown as (○), (X), and (■), respectively.

We compare first the structure functions $F_1(x)$ (from the data of Fig. 10) and $R_1(y_r)$ (from the data of Fig. 19) by plotting the ratios of these functions for events of reaction (1) at 8.05 and 18.5 GeV/c as a function of x and y_r, respectively. Incident-energy independence would correspond to a constant ratio of unity for all values of the variable being considered. [We do not show the ratio for $G_1(y)$ (from the data of Fig. 16) since the kinematic limits for y at the two energies are different and the ratio varies strongly with y.] In Fig. 23(a), we see that the ratio for $F_1(x)$ is close to 1.0 near $x = 0$ but varies significantly as $|x|$ becomes large. In contrast, the ratio for $R_1(y_r)$ as shown in Fig. 23(b) is close to 1.0 everywhere except near $y_r = +1$. The effects near $x = +1$ and $y_r = +1$ can be attributed to the decrease in elastic scattering cross section as the incident momentum increases together with poorer momentum resolution for particles with large laboratory momenta, as noted in Sec. V B.

In Fig. 24, we show the ratios of $F_2(P_T^2)$, $G_2(P_T^2)$, and $R_2(P_T^2)$ at 8.05 and 18.5 GeV/c in reaction (1) as functions of P_T^2. The ratio for $F_2(P_T^2)$ shows a significant dependence on P_T^2 and differs appreciably from unity for most values of P_T^2. The ratios for $G_2(P_T^2)$ and $R_2(P_T^2)$ show smaller variation with P_T^2. However, the ratio for $G_2(P_T^2)$ is significantly less than unity for most values of P_T^2. The ratio for $R_2(P_T^2)$ is close to unity for all but very small P_T^2. Thus the energy independence of the data for reaction (1), especially in the central region, is best exhibited by using the variables y_r and P_T^2. We suggest, therefore, that it would be interesting to study the energy dependence of other inclusive reactions in terms of these variables, to compare with the data presented here.

It is evident that there are particular advantages for each of the sets of variables, i.e., the variables (P_l, P_T^2) evaluated in the rest frame of the target proton, and the c.m. variables (x, P_T^2), (y, P_T^2), and (y_r, P_T^2). No one set displays all the features of inclusive reactions that are relevant to our understanding of strong interaction physics, and the choice of reference frame and of variables depends on the particular theoretical predictions. The advantages of analyzing the data in terms of complementary sets of variables is particularly evident in the present study of the production of negative pions in single-particle inclusive reactions for $\pi^- p$ interactions at 8.05 and 18.5 GeV/c

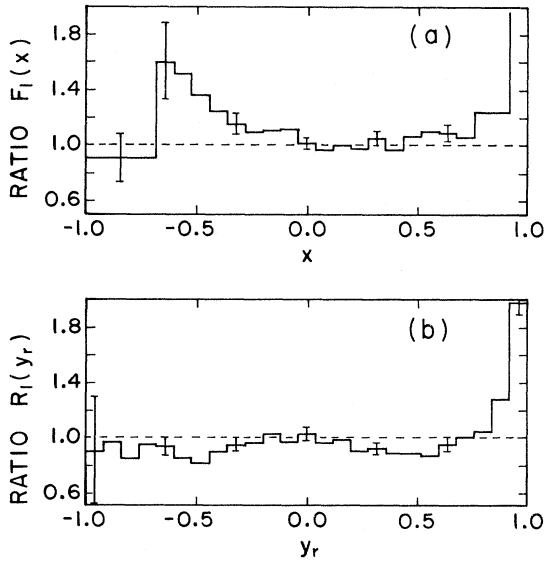

FIG. 23. (a) The ratio of the structure functions $F_1(x)$ for 8.05-GeV/c events to $F_1(x)$ for 18.5-GeV/c events of the reaction $\pi^- + p \to \pi^- +$ anything, as a function of x. (b) The ratio of the structure functions $R_1(y_r)$ for 8.05-GeV/c events to $R_1(y_r)$ for 18.5-GeV/c events of the same reaction, as a function of y_r.

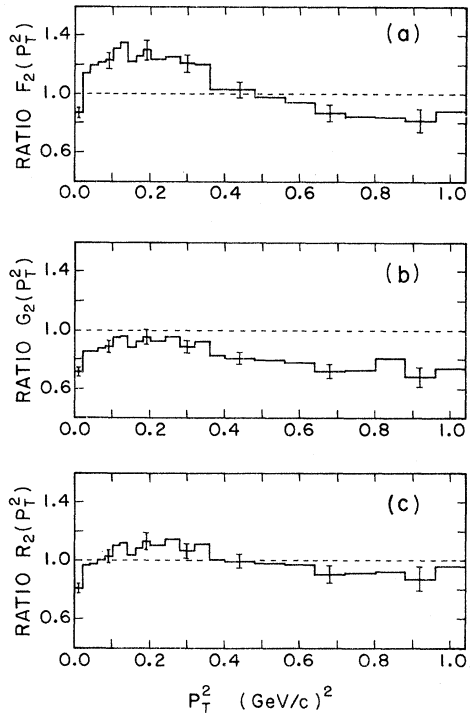

FIG. 24. (a) The ratio of the structure function $F_2(P_T^2)$ for 8.05-GeV/c events to $F_2(P_T^2)$ for 18.5-GeV/c events of the reaction $\pi^- + p \to \pi^- +$ anything as a function of P_T^2. (b) The ratio of the structure function $G_2(P_T^2)$ for 8.05-GeV/c events to $G_2(P_T^2)$ for 18.5-GeV/c events of the same reaction as a function of P_T^2. (c) The ratio of the structure function $R_2(P_T^2)$ for 8.05-GeV/c events to $R_2(P_T^2)$ for 18.5-GeV/c events of the same reaction as a function of P_T^2.

and π^+p interactions at 18.5 GeV/c. Further, by comparing π^+p and π^-p interactions at the same energy, we observe characteristics of πp interactions which depend upon the charge of the incident pion. By simultaneously studying data for π^-p interactions at two different energies, we are able to draw qualitative conclusions about the limiting fragmentation and scaling hypotheses ir this energy range. We look forward to extending this analysis to higher (NAL) energies in the near future.

ACKNOWLEDGMENTS

We would like to thank the staffs of the 80-in. bubble chamber and the AGS at Brookhaven National Laboratory for their cooperation. Dr. D. W. Thomas and R. R. Riley made valuable contributions to this experiment. The cooperation of W. L. Rickhoff, R. L. Erichsen, and the Notre Dame scanning and measuring staff is acknowledged with appreciation.

---

*Research supported in part by the National Science Foundation.

†Present address: Science Applications, Incorporated, Arlington, Virginia 22209. Submitted in partial fulfillment of the requirements for the Ph.D. degree at the University of Notre Dame, Notre Dame, Indiana.

[1]N. N. Biswas, N. M. Cason, V. P. Kenney, J. T. Powers, W. D. Shephard, and D. W. Thomas, Phys. Rev. Lett. 26, 1589 (1971).

[2]W. D. Shephard, J. T. Powers, N. N. Biswas, N. M. Cason, V. P. Kenney, R. R. Riley, D. W. Thomas, J. W. Elbert, and A. R. Erwin, Phys. Rev. Lett. 27, 1164 (1971); 28, 260E (1972).

[3]W. D. Shephard, J. T. Powers, N. N. Biswas, N. M. Cason, V. P. Kenney, and D. W. Thomas, Phys. Rev. Lett. 28, 703 (1972).

[4]M. Alston-Garnjost, K. Barnham, M. S. Rabin, A. Barbaro-Galtieri, S. M. Flatté, J. F. Friedman, G. R. Lynch, J. N. MacNaughton, F. T. Solmitz, C. Risk, W. D. Shephard, J. T. Powers, N. N. Biswas, N. M. Cason, V. P. Kenney, and D. W. Thomas, Phys. Lett. 39B, 402 (1972).

[5]R. P. Feynman, *High Energy Collisions* (Gordon and Breach, New York, 1969), p. 237; Phys. Rev. Lett. 23, 1415 (1969).

[6]K. G. Wilson, Cornell University Report No. CLNS-131, 1970 (unpublished).

[7]C. E. DeTar, Phys. Rev. D 3, 128 (1971).

[8]L. Van Hove, *Proceedings of the Colloquium on Multiparticle Dynamics, University of Helsinki, 1971,* edited by E. Byckling, K. Kajantie, H. Satz, and J. Tuonminiemi (Univ. of Helsinki Press, Helsinki, 1971).

[9]W. R. Frazer, L. Ingber, C. H. Mehta, C. H. Poon, D. Silverman, K. Stowe, P. D. Ting, and H. J. Yesian, Rev. Mod. Phys. 44, 284 (1972).

[10]E. A. Harrington, Ph.D. thesis, University of Notre Dame, 1970 (unpublished).

[11]J. W. Burren and J. Sparrow, Rutherford High Energy Laboratory Report No. NIRL/R/14, 1965 (unpublished).

[12]J. T. Powers, Ph.D. thesis, University of Notre Dame, 1972 (unpublished).

[13]A. H. Mueller, Phys. Rev. D 4, 150 (1971); A. Białas and K. Zalewski, Jagellonian University Report No. TPJW-22/71, 1971 (unpublished).

[14]N. F. Bali, L. S. Brown, R. D. Peccei, and A. Pignotti, Phys. Rev. Lett. 25, 557 (1970).

[15]E. L. Berger and A. Krzywicki, Phys. Rev. Lett. 36B, 380 (1971).

[16]C. Quigg, J. M. Wang, and C. N. Yang, Phys. Rev. Lett. 28, 1290 (1972); C. N. Yang, private communication.

[17]We calculate the right and left multiplicity moments from definitions found in Ref. 16. Some examples are:

$$\langle n_-^R \rangle = \int_0^1 (d\sigma/dx)dx\,,$$

$$\langle n_-^L \rangle = \int_{-1}^0 (d\sigma/dx)dx\,,$$

$$\langle n_-^R (n_-^R - 1)\rangle = \int_0^1 \int_0^1 (d\sigma/dx_1 dx_2)dx_1 dx_2\,,$$

$$\langle n_-^R n_-^L \rangle = \int_0^1 \int_{-1}^0 (d\sigma/dx_1 dx_2)dx_1 dx_2\,.$$

[18]A. Białas and K. Zalewski, Jagellonian University Report No. TPJU-22/71, 1971 (unpublished); Z. Koba, H. B. Nielsen, and P. Olesen, Nucl. Phys. B40, 317 (1972); E. L. Berger, B. Y. Oh, and G. A. Smith, Phys. Rev. Lett. 29. 675 (1972).

[19]Summarized by D. R. O. Morrison, in *Proceedings of the Fourth International Conference on High Energy Collisions, Oxford, England, 1972,* edited by J. R. Smith (Rutherford High Energy Laboratory, Chilton, Didcot, Berkshire, England, 1972), Vol. 1, p. 337.

[20]J. Benecke, T. T. Chou, C. N. Yang, and E. Yen, Phys. Rev. 188, 2159 (1969).

[21]Chan Hong-Mo, H. S. Hsue, C. Quigg, and Jiunn-Ming Wang, Phys. Rev. Lett. 26, 672 (1971).

[22]E. W. Anderson, E. J. Bleser, C. B. Collins, T. Fujii, J. Menes, F. Turkot, R. A. Corrigan, Jr., R. M. Edelstein, N. C. Hien, T. J. McMahon, and I. Nadelhaft, Phys. Rev. Lett. 16, 855 (1966); V. Amaldi, R. Biancastelli, C. Bosio, G. Matthiae, J. V. Allaby, A. N. Diddens, R. W. Robinson, A. Klovning, J. Litt, L. S. Rochester, K. Schlupmann, and A. M. Wetherell, Phys. Lett. 34B, 435 (1971).

[23]H. D. I. Abarbanel, Phys. Lett. 34B, 69 (1971).